Supporting Information

Pincer-type pyridylidene amide complexes with the first row transition metals nickel, cobalt and zinc

Philipp Melle, Nathalie Ségaud, and Martin Albrecht*

Department für Chemie und Biochemie, Universität Bern, Freiestrasse 3, CH–3012 Bern, Switzerland.

*email: martin.albrecht@dcb.unibe.ch

Table of contents:

1. ORTEP structures of complexes 2b, 2c, 3b, 3c

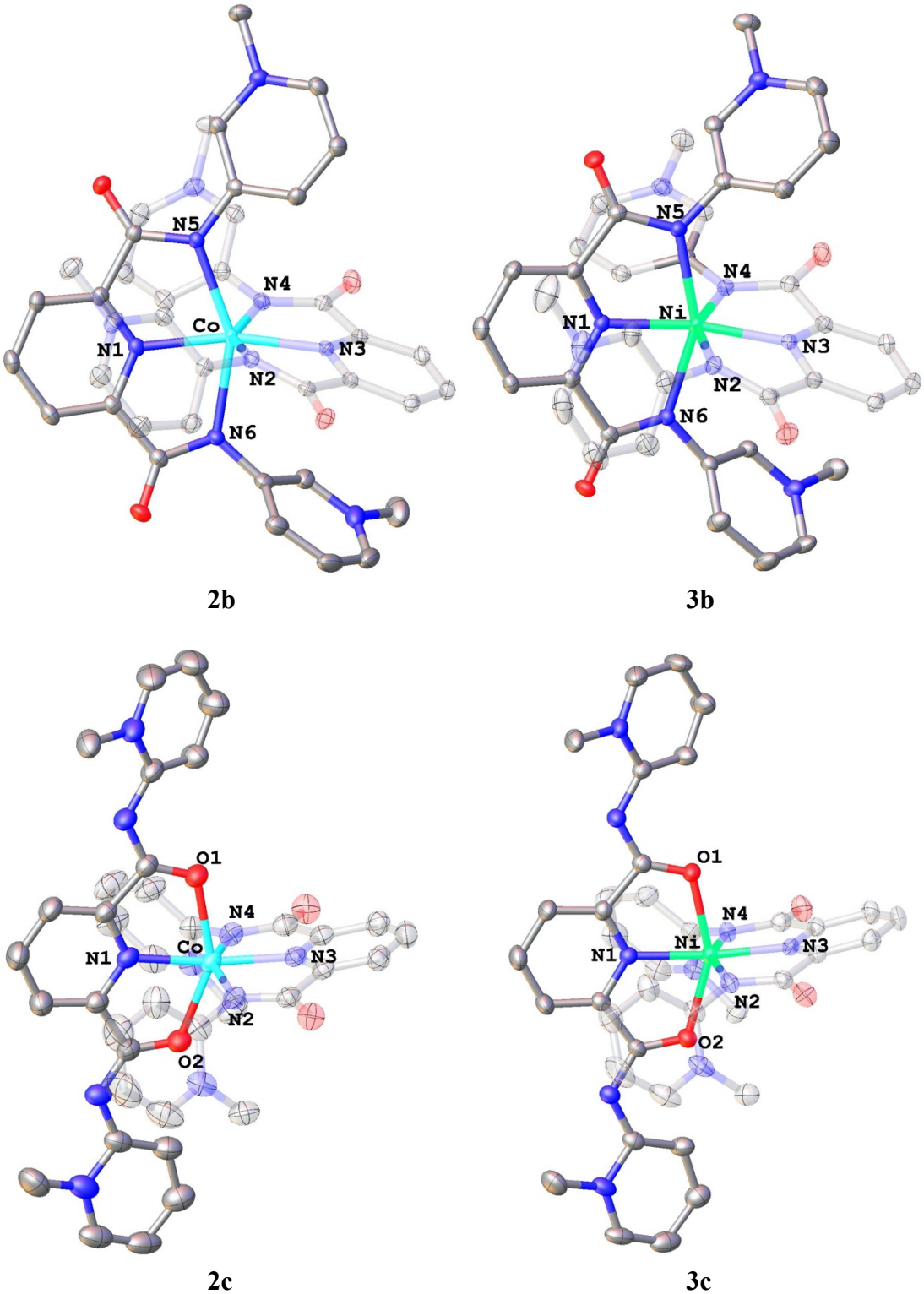

Figure S1. ORTEP representations of complex cations of **2b**, **2c**, **3b**, and **3c**; all ellipsoids at 50% probability level (hydrogen atoms and co-crystallized solvent molecules omitted for clarity).

Table S1. Selected bond lengths (Å) and angles (deg) of complex cations 2b–c and 3b–c.

	2b (M = Co)	**2c (M = Co)**	**3b (M = Ni)**	**3c (M = Ni)**
M–N2	2.160(2)	2.141(2)	2.136(2)	2.096(3)
M–N3	2.036(2)	2.029(2)	1.997(2)	1.983(3)
M–N4	2.137(2)	2.123(3)	2.125(2)	2.119(4)
N2–M–N4	149.6(2)	151.4(2)	152.9(1)	154.5(2)
M–E1 [a]	2.196(2)	2.190(2)	2.181(2)	2.191(3)
M–N1	2.033(2)	2.043(2)	1.992(2)	1.990(3)
M–E2 [a]	2.205(2)	2.217(2)	2.183(3)	2.158(3)
E1–M–E2 [a]	151.5(1)	149.6(2)	153.6(2)	153.7(1)

[a] E1 = N5 and E2 = N6 for **2b** and **3b**; E = O for **2c** and **3b**.

2. Synthesis and characterization of [Ru(*ortho*-pyPYA$_2$)(MeCN)$_3$](PF$_6$)$_2$

Synthetic procedure: A solution of the *ortho*-pyPYA$_2$ ligand (260 mg, 0.4 mmol), [Ru(η^6-*p*-cymene)Cl$_2$]$_2$ (120 mg, 0.2 mmol) and Na_2CO_3 (130 mg, 1.2 mmol) in MeCN (100 mL) was stirred at reflux for 16 h. The reaction mixture changed colour from orange to deep red. After cooling to r.t., the reaction mixture was filtered over Celite and the red solution was concentrated under reduced pressure to 5 mL. Addition of Et_2O (100 mL) gave a dark red precipitate which was collected by filtration and redisolved in MeCN (10 mL), filtered over Celite and precipitated again by addition of Et_2O (100 mL). The crude product was purified chromatographically (MeCN, AlOx) and drying under reduced pressure yielded complex [Ru(*ortho*-pyPYA$_2$)(MeCN)$_3$](PF$_6$)$_2$ as an orange-red powder (150 mg, 45% yield). ^{1}H NMR (300 MHz, DMSO-d_6) δ 8.78 (d, J = 6.0 Hz, 2H, H_{PYA}), 8.41–8.31 (m, 2H, H_{PYA}), 8.28–8.23 (m, 3H, H_{pyr}), 7.72 (t, J = 7.1 Hz, 2H, H_{PYA}), 7.57 (t, J = 7.1 Hz, 2H, H_{PYA}), 3.96 (s, 6H, N-CH_3), 2.44 (s, 3H, NCCH_3), 2.40 (s, 6H, NCCH_3). ^{13}C NMR (75 MHz, DMSO-d_6) δ 169.5 (CO), 159.6 (C_{PYA}), 155.1 (C_{pyr}), 144.7 (CH_{PYA}), 144.5 (CH_{PYA}), 137.2 (CH_{pyr}), 126.9 (CH_{pyr}), 126.2 (CH_{PYA}), 121.2 (CH_{PYA}), 43.6 (NCH_3), 3.5 (NCCH_3), 3.1 (NCCH_3). HR ESI-MS: m/z calculated for $C_{23}H_{23}O_2N_7F_6PRu$ $[M–PF_6]^+$ = 717.0870; found: 717.09. Elemental Analysis: anal. calculated for $C_{25}H_{26}F_{12}N_8O_2P_2Ru$: C: 34.85; H: 3.04; N: 13.01. Found: C: 34.48; H: 2.56; N: 12.92.

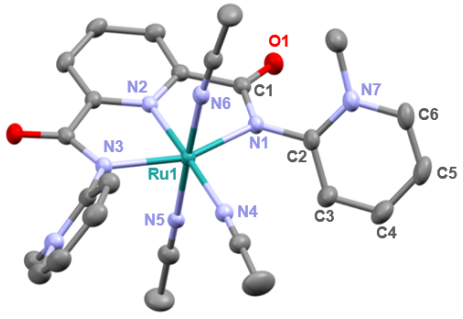

Figure S2. ORTEP representation of [Ru(κ^3-*N,N,N-ortho*-pyPYA$_2$)(MeCN)$_3$]; all ellipsoids at 50% probability level (hydrogen atoms and co-crystallized solvent molecules omitted).

3. Isomerization of [Zn(*ortho*-pyPYA$_2$)$_2$](PF$_6$)$_2$ complex 6c

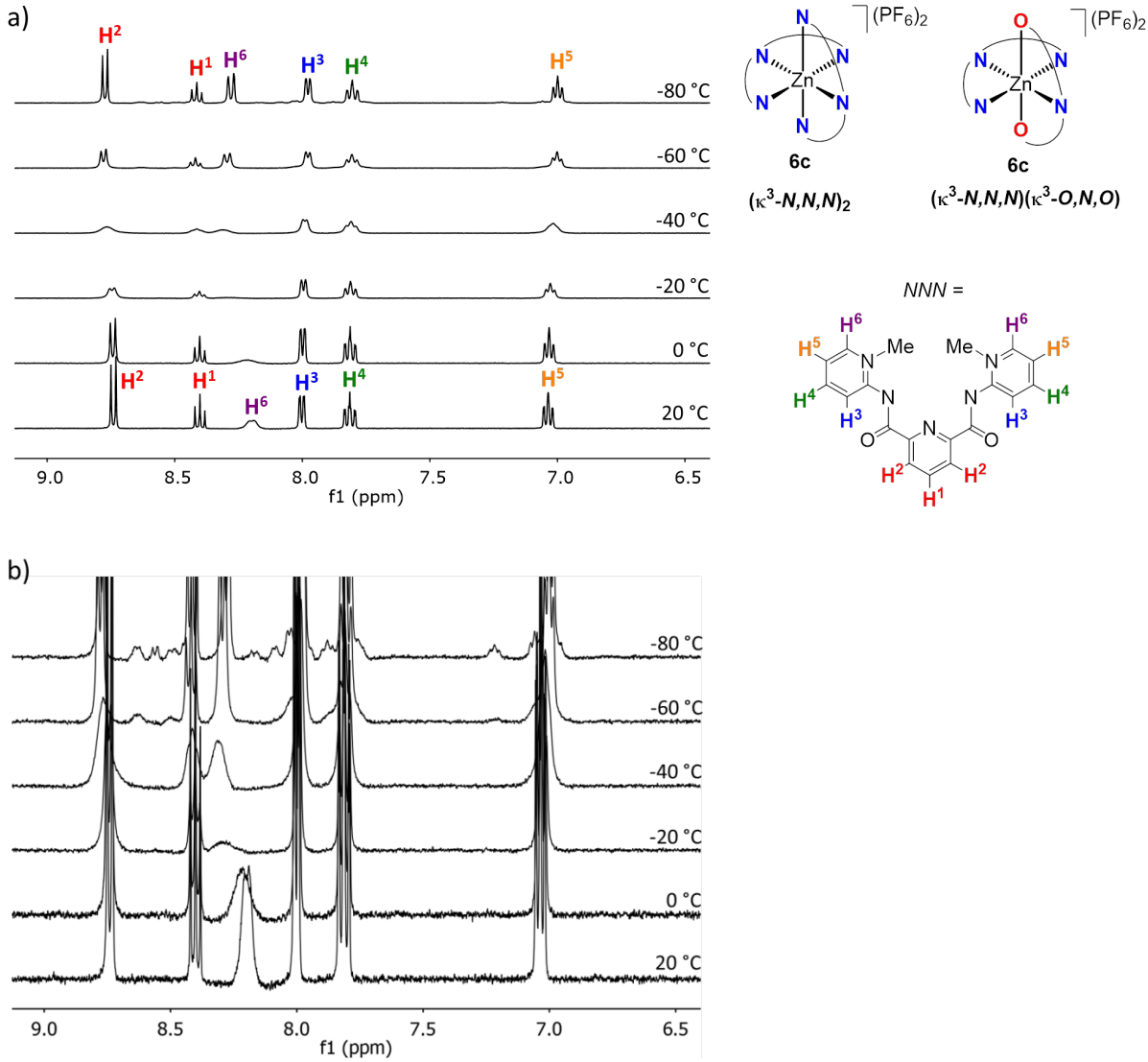

Figure S3. a) Aromatic area between 9 and 6.5 ppm of temperature-dependent ^{1}H NMR spectra of [Zn(*ortho*-pyPYA$_2$)$_2$](PF$_6$)$_2$ **6c** (400 MHz, CD_2Cl_2 solution) recorded from +20 °C to –80 °C; b) Same spectral range with larger intensity to identify minor species.

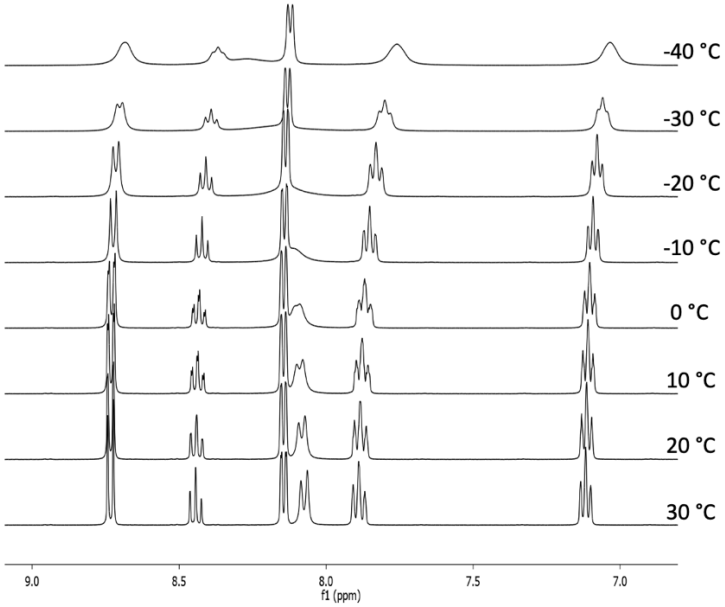

Figure S4. a) Aromatic area between 9 and 6.5 ppm of temperature-dependent ^{1}H NMR spectra of [Zn(*ortho*-pyPYA$_2$)$_2$](PF$_6$)$_2$ **6c** (400 MHz) in CD_3CN solution, recorded from +30 °C to –40 °C, indicating essentially identical dynamic processes as observed in CD_2Cl_2 (see Fig. S3). However, decoalescence temperature is not reached due to the higher melting point of CD_3CN.

Table S2. Chemical shifts of pyridyl and PYA protons for the two different coordination isomers of [Zn(*ortho*-pyPYA$_2$)$_2$](PF$_6$)$_2$ complex **6c** (–80°C, CD_2Cl_2, 400 MHz), difference of the resonance frequencies δν, coalescence temperature T_c and energy barrier $\Delta G^{‡}$ for the isomerization process.

		δ_H (–80 °C) [ppm]						
entry	proton	(κ^3-*N,N,N*)$_2$	(κ^3-*N,N,N*)/(κ^3-*O,N,O*)			$\delta\nu$ [Hz]	T_c [K]	$\Delta G^{‡}$ [kcal/mol]
			kN	*κO*	Ø			
1[a]	H^1_{pyr}	8.41	-	-	-	-	233	-
2	H^2_{pyr}	8.77	8.63	8.56	8.60	65	233	11.2
3	H^3_{PYA}	7.98	8.09	8.17	8.13	60	233	11.2
4	H^4_{PYA}	7.80	7.77	7.88	7.83	50	233	11.3
5	H^5_{PYA}	7.00	7.06	7.22	7.14	55	233	11.3
6	H^6_{PYA}	8.28	8.03	8.03	8.03	100	253	11.9
7 (average)								11.4 ± 0.3

[a]assignment of H^1_{pyr} protons in minor species impossible due to overlap of resonances.

4. IR spectra of all compounds.

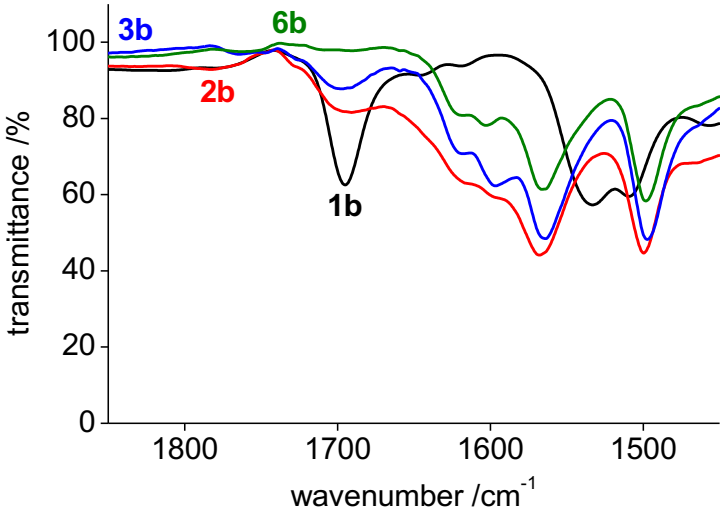

Figure S5. IR spectra of *meta*-pyPYA$_2$ pincer series.

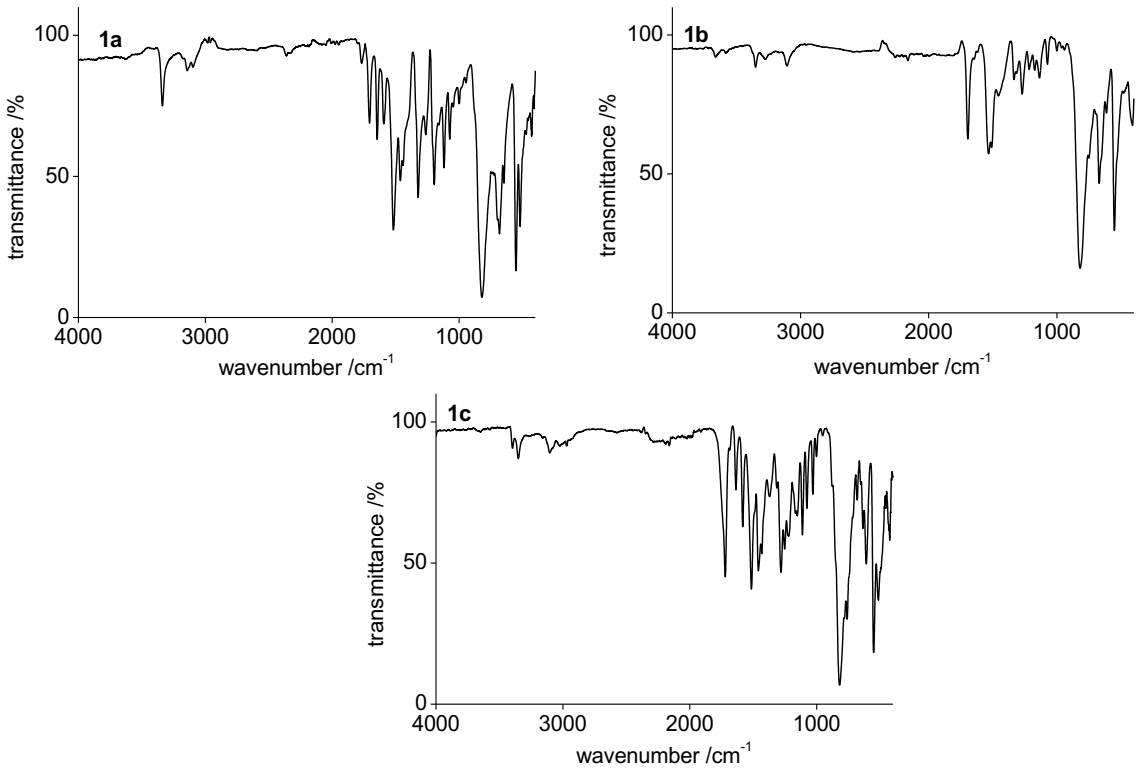

Figure S6. IR spectra of *para*- *meta*- and *ortho*-pyPYA$_2$ ligands **1a–c**.

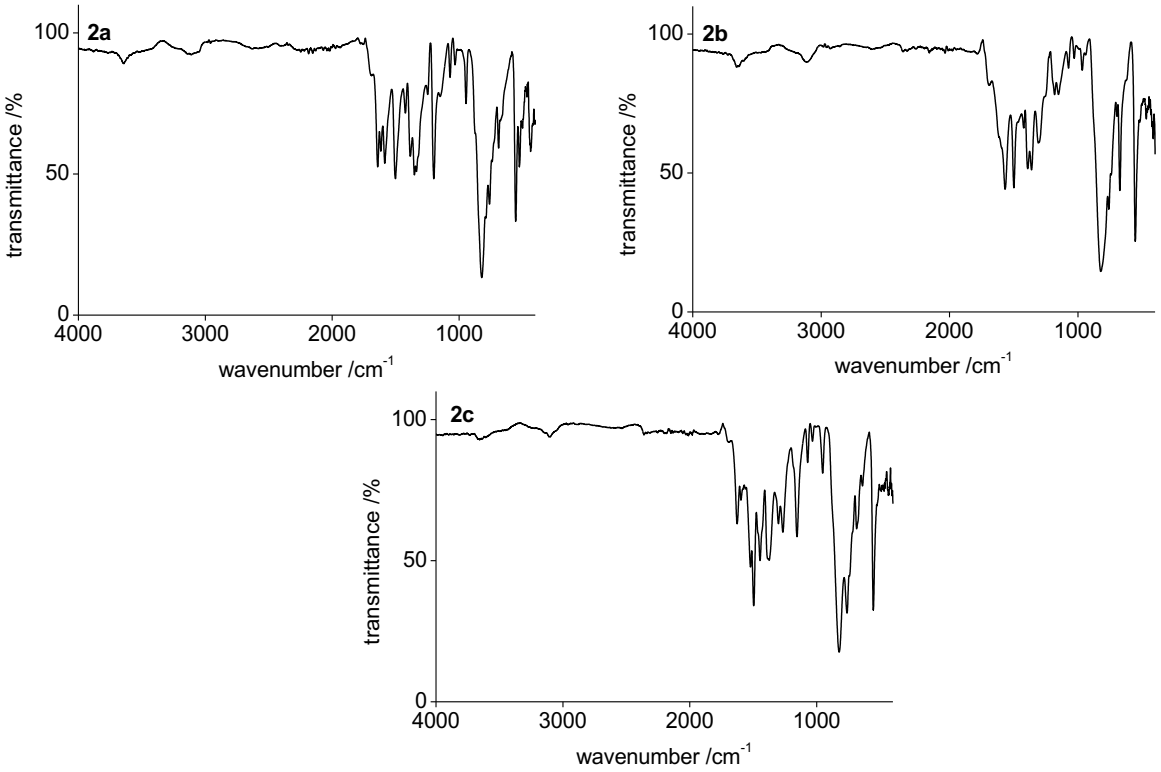

Figure S7. IR spectra of $[Co(pyPYA_2)_2](PF_6)_2$ complexes **2a–c**.

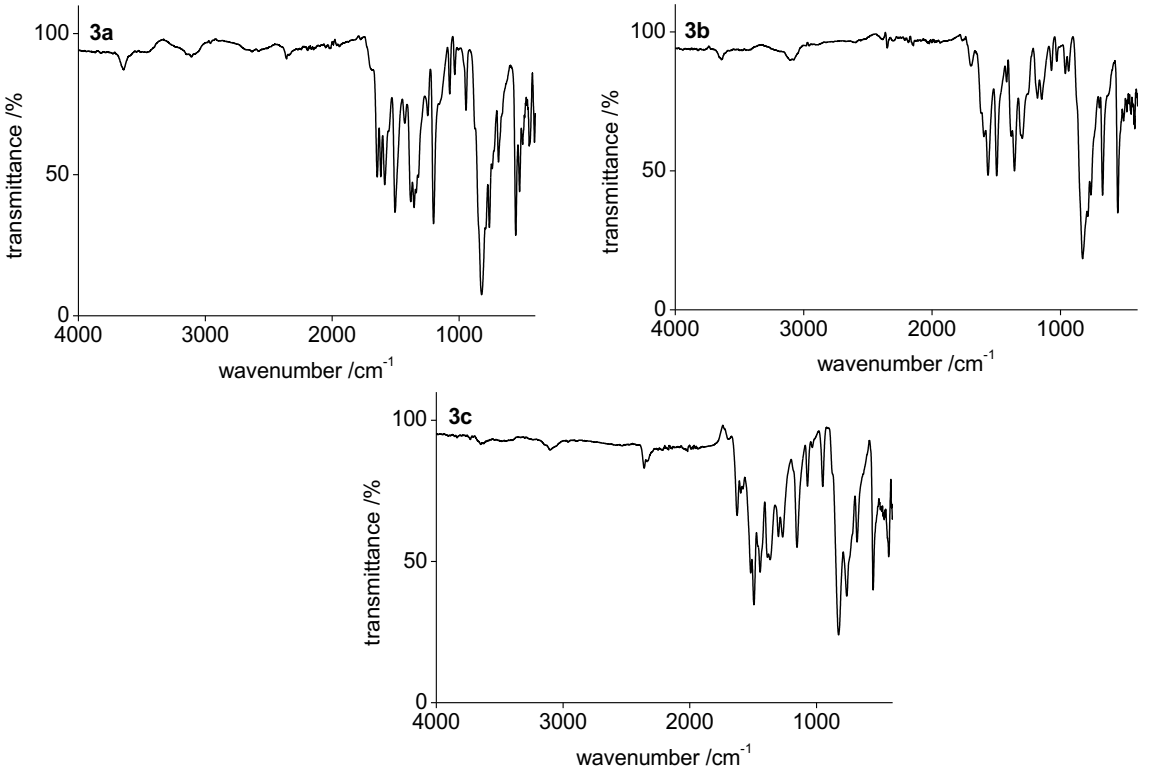

Figure S8. IR spectra of $[Ni(pyPYA_2)_2](PF_6)_2$ complexes **3a–c**.

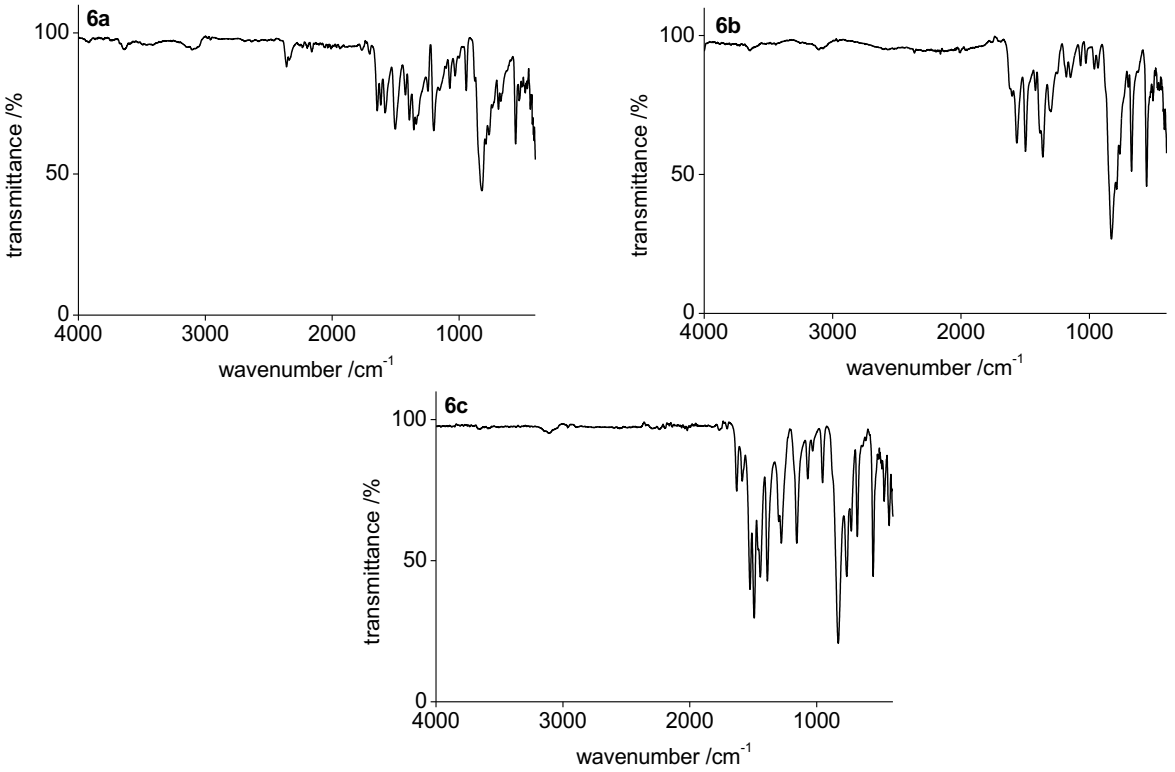

Figure S9. IR spectra of $[Ni(pyPYA_2)_2](PF_6)_2$ complexes **6a–c**.

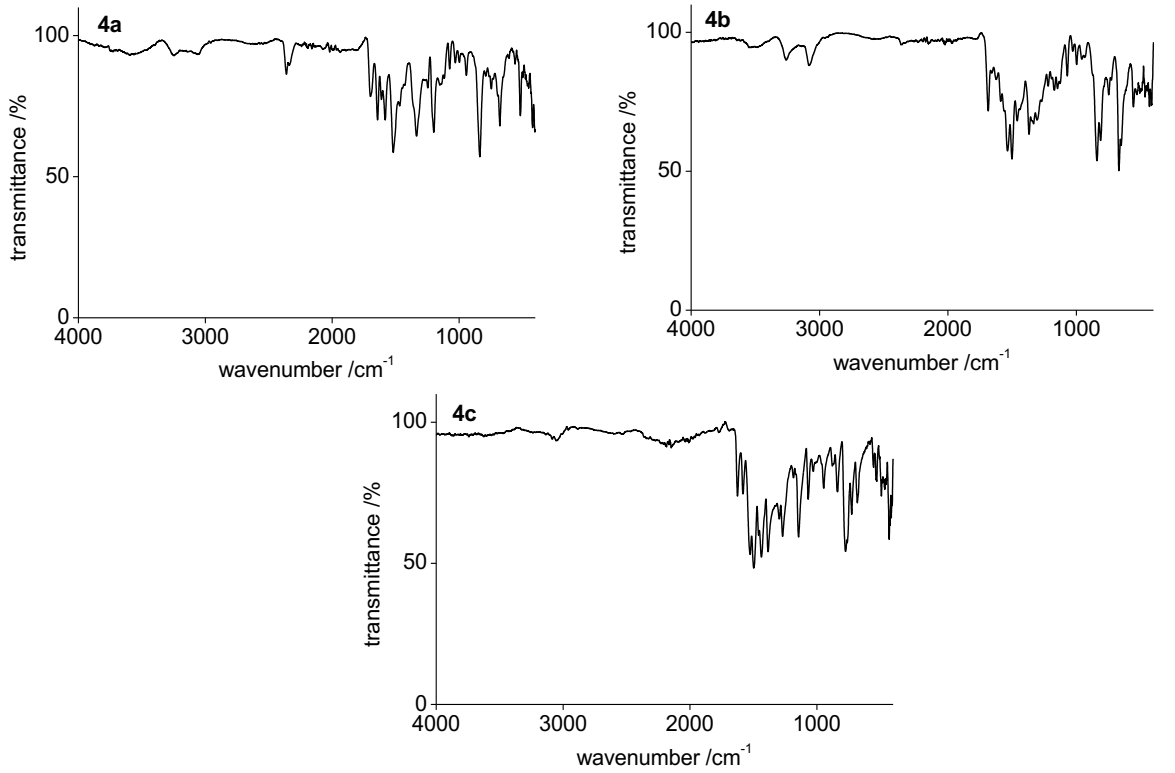

Figure S10. IR spectra of $[Co(pyPYA_2)Cl_2]$ complexes **4a–c**.

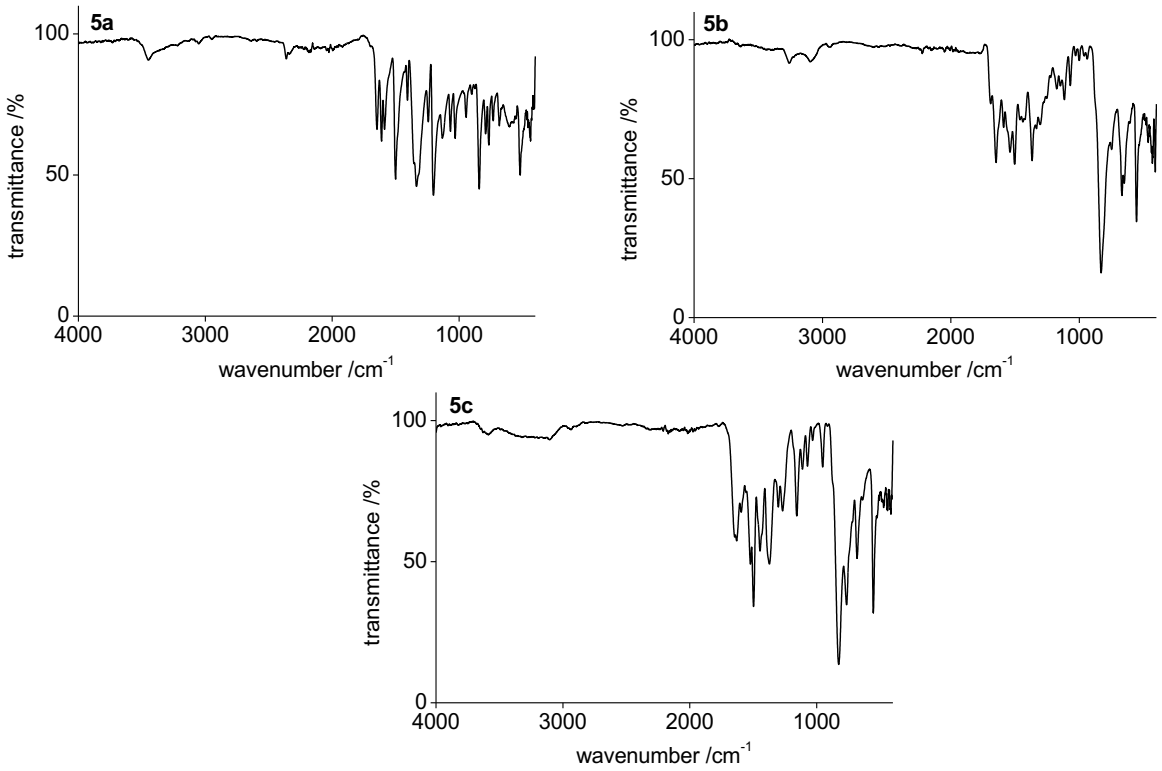

Figure S11. IR spectra of [Ni(pyPYA$_2$)Cl$_2$] complexes **5a–c**.

5. Cyclic voltammetry measurements

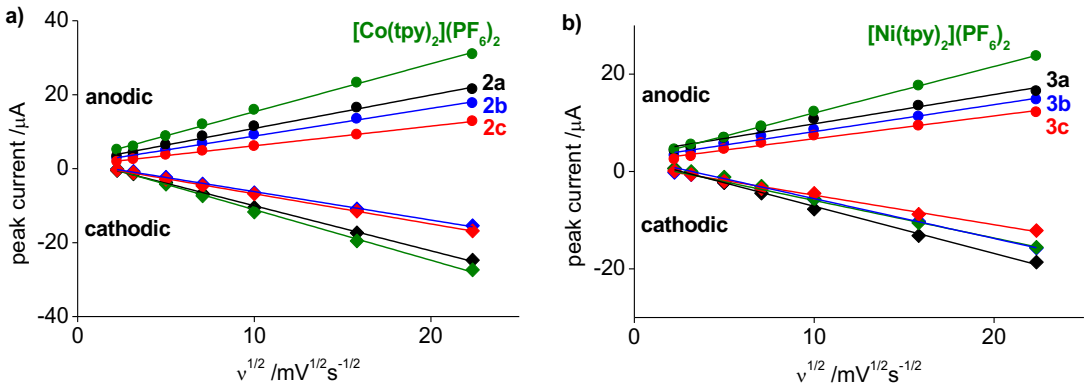

Figure S12. Linear dependence of redox peak current on the square root of the scan rate: a) cobalt complex series (R > 0.99); b) nickel complex series (R > 0.98); [M(terpy)$_2$](PF$_6$)$_2$ green curves; [M(*para*-pyPYA$_2$)$_2$](PF$_6$)$_2$ black curves; [M(*meta*-pyPYA$_2$)$_2$](PF$_6$)$_2$ blue curves; [M(*ortho*-pyPYA$_2$)$_2$](PF$_6$)$_2$ red curves.

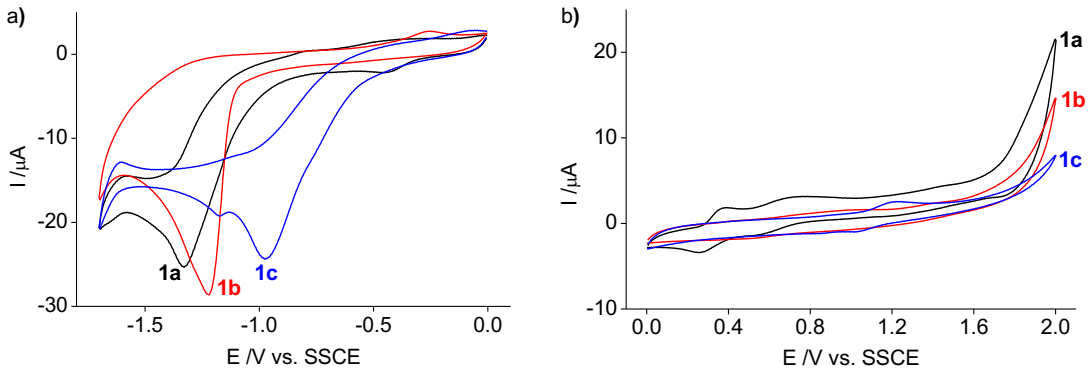

Figure S13. Cyclic voltammetry measurements of pyPYA$_2$ ligands **1a–c** in MeCN: a) negative potential range: –1.7 to 0 V; b) positive potential range: 0 to +2 V. Conditions: 10 mL solvent, 1 mM sample and 100 mM (*n*Bu$_4$N)PF$_6$ as supporting electrolyte at 100 mVs^{-1} scan rate (potentials vs. SSCE using the Fc$^+$/Fc couple as standard; E$_{1/2}$ = +0.4319).

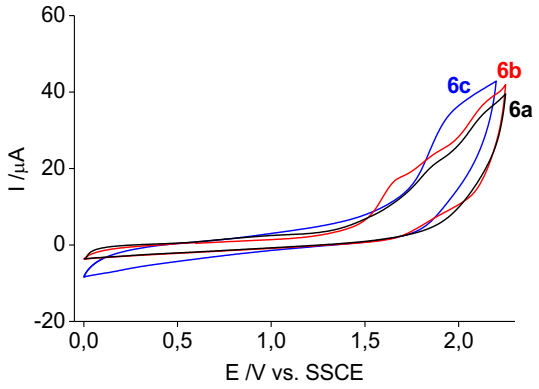

Figure S14. Cyclic voltammetry measurements of complexes **6a–c** in MeCN; **6a** [Zn(*para*-pyPYA$_2$)$_2$](PF$_6$)$_2$ in black; **6b** [Zn(*meta*-pyPYA$_2$)$_2$](PF$_6$)$_2$ in blue; **6c** [Zn(*ortho*-pyPYA$_2$)$_2$](PF$_6$)$_2$ in red. Conditions: 10 mL solvent, 1 mM sample and 100 mM (*n*Bu$_4$N)PF$_6$ as supporting electrolyte at 100 mVs^{-1} scan rate (potentials vs. SSCE using the Fc$^+$/Fc couple as standard; E$_{1/2}$ = +0.4319).

6. Deuterium incorporation in PYA pyridinium in complex $2b^+$

Table S3. Cationic complex species observed in HR ESI-MS analysis for **2b**, $\mathbf{2b}^+$ and $\mathbf{2b}^+$-d_8.

	2b	$\mathbf{2b}^+$	$\mathbf{2b}^+$-d_8
	$[Co(meta\text{-}pyPYA_2)_2](PF_6)_2$	$[Co(meta\text{-}pyPYA_2)_2](PF_6)_3$	$[Co(meta\text{-}pyPYA_2\text{-}d_4)_2](PF_6)_3$
$[M–PF_6]^+$	898.1740	1043.1393	1051.1883
$[M–2PF_6]^{2+}$	376.6044	449.0865	453.1108
$[M–3PF_6]^{3+}$	not detected	251.0696	253.7526

^{1}H NMR analysis of complexes $2b^+$ and $2b^+$-d_8

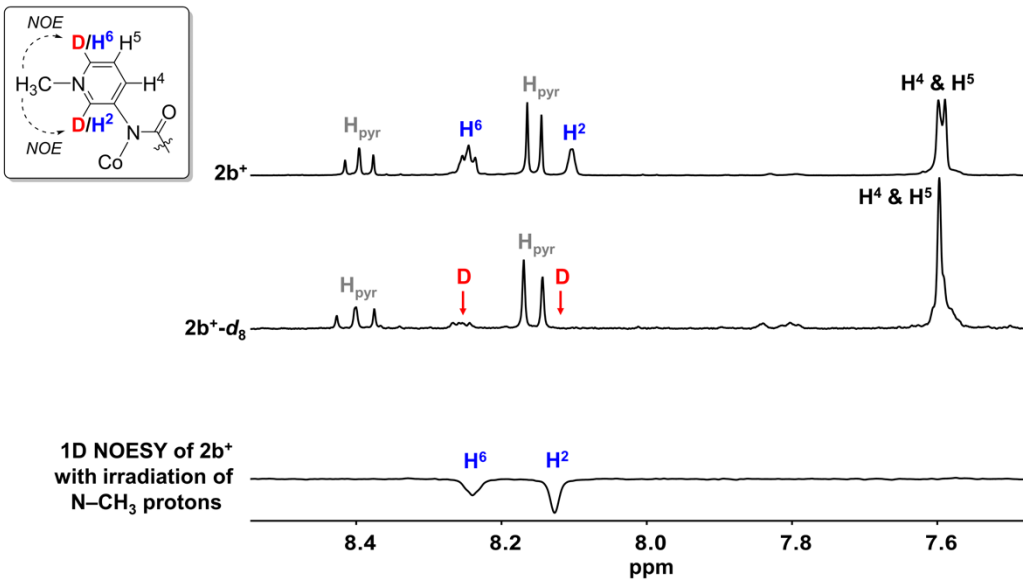

Figure S15. ^{1}H NMR spectra of complex $\mathbf{2b}^+$ (top) and $\mathbf{2b}^+$-d_8 (middle) in MeCN-d_3. Showing deuterium incorporation in H^2 and H^6 position of the PYA pyridinium. Assignment of PYA pyridinium protons with help of 1D NOESY experiment (bottom) with selective irradiation of N–CH_3 protons.

7. ^{1}H and ^{13}C NMR spectra of Zn-complexes 6a–c

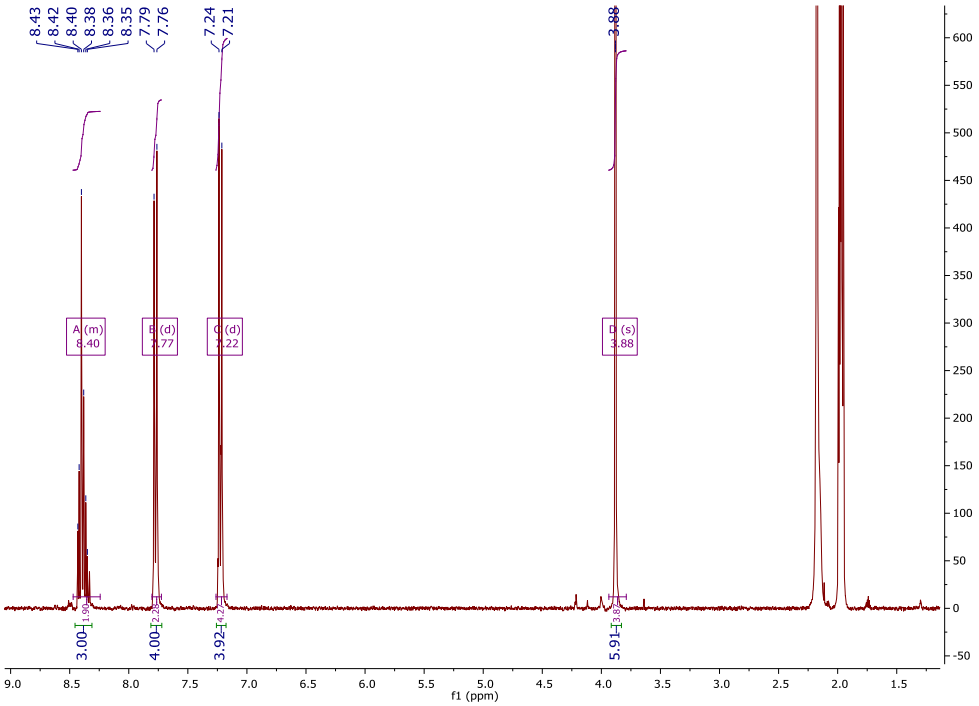

Figure S16. ^{1}H NMR spectrum of complex **6a** (300 MHz, CD_3CN, 298 K).

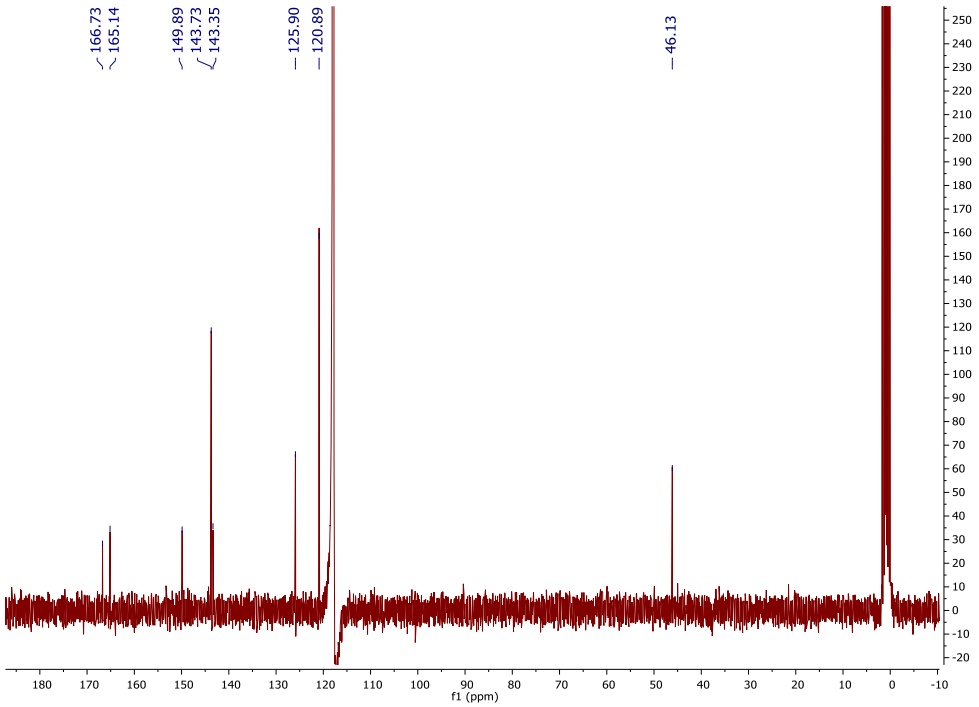

Figure S17. ^{13}C NMR spectrum of complex **6a** (75 MHz, CD_3CN, 298 K).

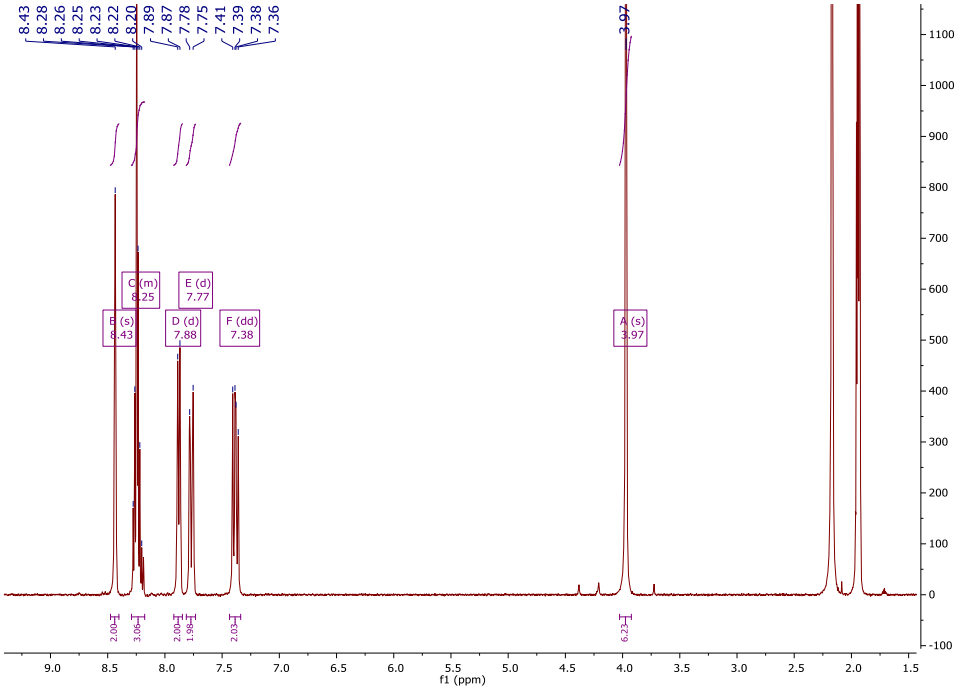

Figure S18. ^{1}H NMR spectrum of complex **6b** (300 MHz, CD_3CN, 298 K).

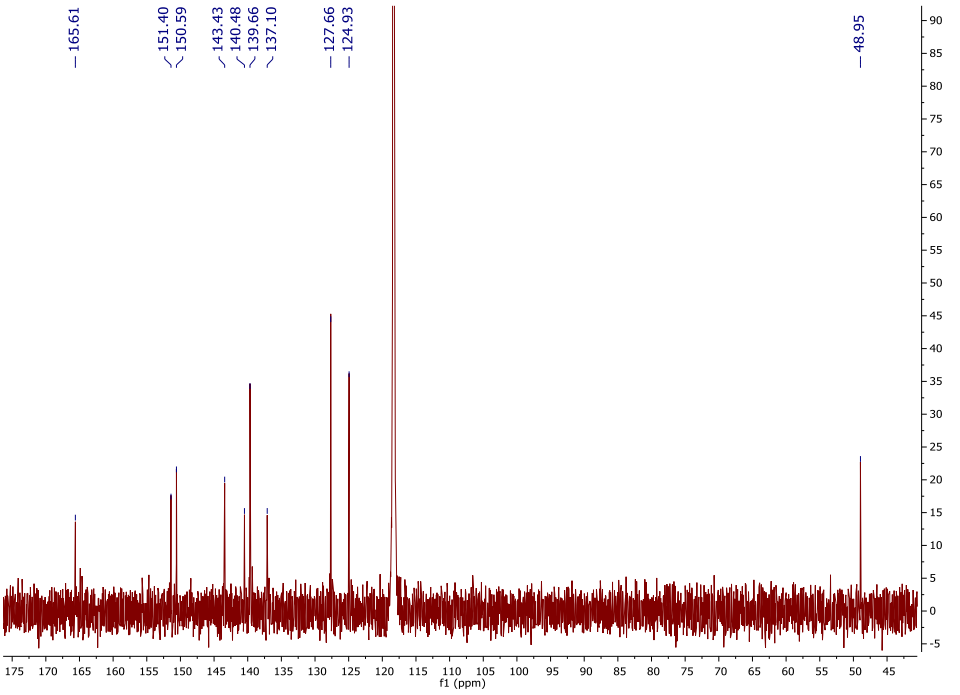

Figure S19. ^{13}C NMR spectrum of complex **6b** (75 MHz, CD_3CN, 298 K).

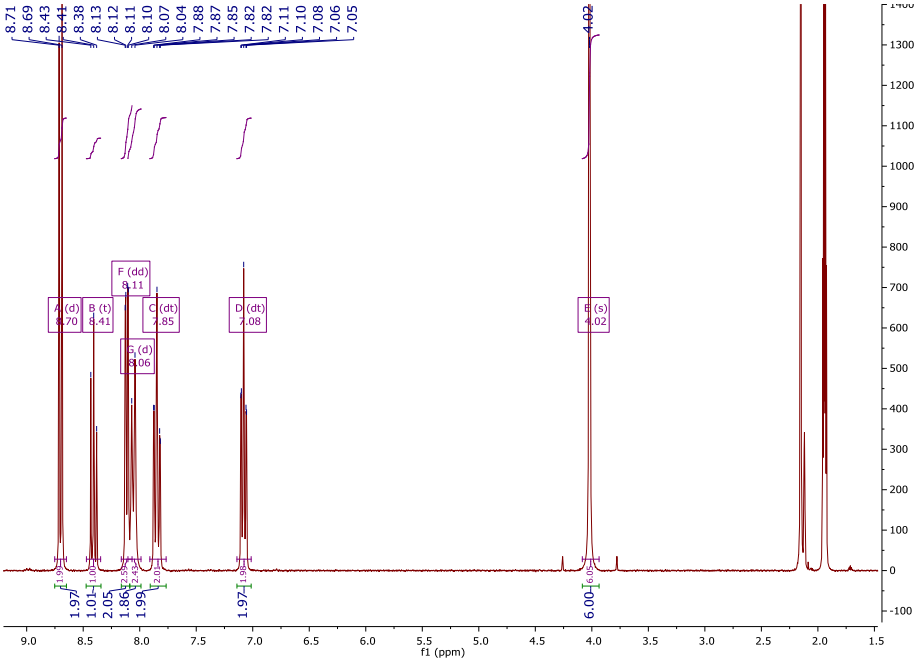

Figure S20. ^{1}H NMR spectrum of complex **6c** (300 MHz, CD_3CN, 298 K).

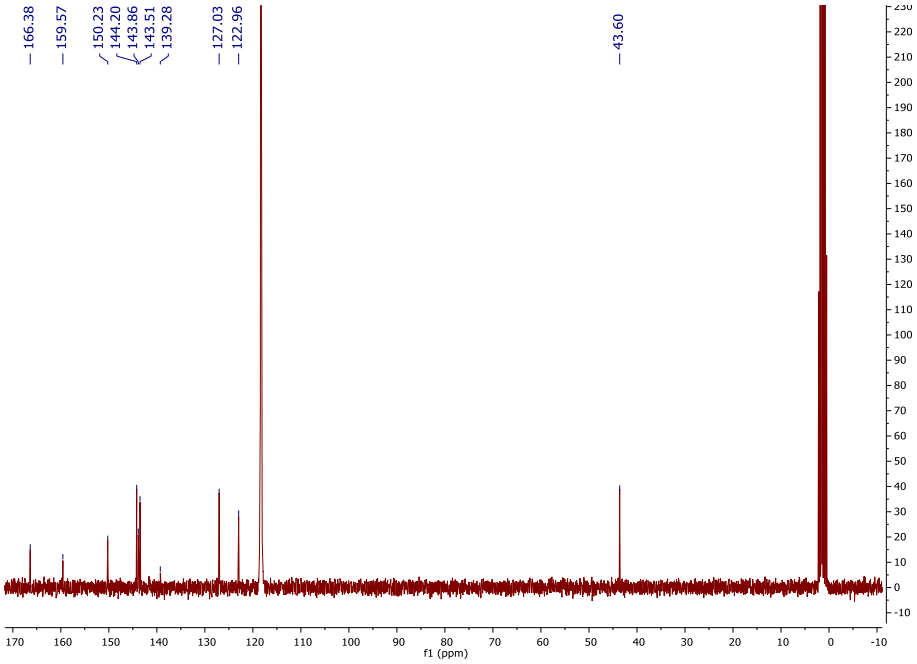

Figure S21. ^{13}C NMR spectrum of complex **6c** (75 MHz, CD_3CN, 298 K).

8. Crystallographic details

Table S4. Crystal data and structure refinement for complexes **2b**, **2b**$^{+}$ and **3b**.

complex	**2b**	**2b**$^{+}$	**3b**
CCDC No	2015875	2015876	2015878
Empirical formula	$C_{44}H_{43}CoF_{12}N_{13}O_4P_2$	$C_{38}H_{38}CoF_{18}N_{10}O_6P_3$	$C_{44}H_{43}F_{12}N_{13}NiO_4P_2$
Formula weight	1166.78	1224.62	1166.56
Temperature/K	123(2)	173.00(10)	123(2)
Wavelength /Å	0.71073 (MoKα)	0.71073 (MoKα)	0.71073 (MoKα)
Crystal system	triclinic	monoclinic	triclinic
Space group	*P*-1	$P2_1/c$	*P*-1
a/Å	12.5415(4)	13.05781(13)	12.5126(3)
b/Å	13.9618(4)	14.7905(2)	13.9713(4)
c/Å	15.2652(4)	24.4665(3)	15.2848(4)
α/°	67.212(3)	90	67.053(2)
β/°	82.957(2)	99.3165(10)	82.782(2)
γ/°	83.194(2)	90	82.793(2)
Volume /Å^3	2438.35(13)	4662.91(10)	2432.53(12)
Z	2	4	2
Density (calculated) /Mg/m^3	1.589	1.744	1.593
Absorption coefficient /mm^{-1}	0.522	0.602	0.569
F(000)	1190	2472	1192
Crystal size /mm^3	0.332 x 0.082 x 0.043	0.3 × 0.05 × 0.05	0.272 x 0.068 x 0.046
Theta range for data collection	1.587 to 28.22°	3.16 to 54.098°	1.588 to 28.176°
Index ranges	$-16 \le h \le 16$ $-18 \le k \le 18$ $-19 \le l \le 19$	$-16 \le h \le 16$ $-18 \le k \le 18$ $-23 \le l \le 31$	$-16 \le h \le 16$ $-18 \le k \le 17$ $-20 \le l \le 20$
Reflections collected	44161	39769	48509
Independent reflections	11003 [R_{int} = 0.0442]	10068 [R_{int} = 0.0427, R_{sigma} = 0.0450]	11031 [R_{int} = 0.0503]
Data / restraints / parameters	11003 / 63 / 692	10068 / 3 / 699	11031 / 0 / 692
Goodness-of-fit on F^2	1.026	1.102	1.027
Final R indices [I>2sigma(I)]	R_1 = 0.0497 wR_2 = 0.1136	R_1 = 0.0584 wR_2 = 0.1544	R_1 = 0.0509 wR_2 = 0.1118
R indices (all data)	R_1 = 0.067 wR_2 = 0.1237	R_1 = 0.0816 wR_2 = 0.1661	R_1 = 0.0731 wR_2 = 0.1239
Largest diff. peak and hole /e.Å^{-3}	2.21 and -0.72	1.28 and -0.80	1.783 and -0.652

Table S5. Crystal data and structure refinement for complexes **2c** and **3c**.

complex	**2c**	**3c**	[Ru(*ortho*-pyPYA$_2$)(MeCN)$_3$](PF$_6$)$_2$
CCDC No	2015877	2015879	2015883
Empirical formula	$C_{38}H_{34}CoF_{12}N_{10}O_4P_2$	$C_{38}H_{34}F_{12}N_{10}NiO_4P_2$	$C_{29}H_{32}F_{12}N_{10}O_2P_2Ru$
Formula weight	1043.62	1043.40	943.65
Temperature/K	173.01(10)	173.00(10)	123(2)
Wavelength /Å	0.71073 (MoKα)	0.71073 (MoKα)	0.71073 (MoKα)
Crystal system	monoclinic	monoclinic	triclinic
Space group	$P2_1/n$	$P2_1/n$	P -1
a/Å	11.94056(17)	11.9760(2)	12.4959(3)
b/Å	21.9377(4)	21.8343(3)	12.8519(4)
c/Å	16.2425(2)	16.1933(2)	13.2986(3)
α/°	90	90	77.984(2)
β/°	93.1440(13)	92.2670(10)	77.089(2)
γ/°	90	90	64.978(2)
Volume /Å^3	4248.28(12)	4231.03(11)	1870.64(9)
Z	4	4	2
Density (calculated) /Mg/m^3	1.632	1.638	1.675
Absorption coefficient /mm^{-1}	0.587	0.642	0.609
F(000)	2116.0	2120.0	948
Crystal size /mm^3	0.462 × 0.348 × 0.163	0.15 × 0.05 × 0.05	0.253 x 0.197 x 0.059
Theta range for data collection	3.122 to 56.388°	3.132 to 56.302	1.584 to 28.265
Index ranges	-15 ≤ h ≤ 15 -29 ≤ k ≤ 29 -21 ≤ l ≤ 20	-14 ≤ h ≤ 15 -28 ≤ k ≤ 27 -21 ≤ l ≤ 20	-16<=h<=16 -16<=k<=16 -17<=l<=17
Reflections collected	73492	36391	47400
Independent reflections	9855 [R_{int} = 0.0471, R_{sigma} = 0.0263]	9541 [R_{int} = 0.0777, R_{sigma} = 0.0843]	8603 [R_{int} = 0.0321]
Data / restraints / parameters	9855 / 618 / 727	9541 / 0 / 608	8603 / 738 / 640
Goodness-of-fit on F^2	1.117	1.021	1.074
Final R indices [I>2sigma(I)]	R_1 = 0.0585 wR_2 = 0.1509	R_1 = 0.0651 wR_2 = 0.1344	R_1 = 0.0319 wR_2 = 0.0796
R indices (all data)	R_1 = 0.0702 wR_2 = 0.1581	R_1 = 0.1133 wR_2 = 0.1578	R_1 = 0.0361 wR_2 = 0.0824
Largest diff. peak and hole /e.Å^{-3}	1.17 and -0.74	0.65 and -0.60	0.816 and -0.466

Table S6. Crystal data and structure refinement for complexes **4a–c**.

complex	**4a**	**4b**	**4c**
CCDC No	2015880	2015881	2015882
Empirical formula	$C_{19}H_{19}Cl_2CoN_5O_3$	$C_{19}H_{19}Cl_2CoN_5O_3$	$C_{19}H_{17}Cl_2CoN_5O_2$
Formula weight	633.46	495.22	477.20
Temperature/K	173.01(10)	123(2)	173.00(10)
Wavelength /Å	1.54184 (CuKα)	0.71073 (MoKα)	0.71073 (MoKα)
Crystal system	monoclinic	monoclinic	triclinic
Space group	*I*2/*a*	C2/c	P-1
a/Å	20.84210(10)	17.4295(4)	7.9978(2)
b/Å	13.98040(10)	14.5425(3)	9.2730(2)
c/Å	19.00770(10)	7.9196(2)	14.4181(4)
α/°	90	90	102.016(2)
β/°	95.0990(10)	100.252(2)	99.280(2)
γ/°	90	90	104.188(2)
Volume /Å^3	5516.56(6)	1975.32(8)	988.23(4)
Z	8	4	2
Density (calculated) /Mg/m^3	1.525	1.665	1.604
Absorption coefficient /mm^{-1}	8.409	1.173	1.165
F(000)	2616.0	1012	486.0
Crystal size /mm^3	0.2 × 0.05 × 0.05	0.22 x 0.17 x 0.04	0.15 × 0.1 × 0.05
Theta range for data collection	7.624 to 154.284	1.836 to 28.138°	4.69 to 56.206°
Index ranges	$-26 \le h \le 26$ $-16 \le k \le 17$ $-17 \le l \le 23$	$-22 \le h \le 22$ $-19 \le k \le 18$ $-10 \le l \le 10$	$-10 \le h \le 10$ $-12 \le k \le 12$ $-18 \le l \le 18$
Reflections collected	27154	10573	16903
Independent reflections	5678 [R_{int} = 0.0431, R_{sigma} = 0.0310]	2251 [R_{int} = 0.0258]	4480 [R_{int} = 0.0382, R_{sigma} = 0.0376]
Data / restraints / parameters	5678 / 0 / 340	2251 / 1 / 143	4480 / 0 / 264
Goodness-of-fit on F^2	1.043	1.038	1.033
Final R indices [I>2sigma(I)]	R_1 = 0.0339 wR_2 = 0.0833	R_1 = 0.0260 wR_2 = 0.0653	R_1 = 0.0333 wR_2 = 0.0707
R indices (all data)	R_1 = 0.0373 wR_2 = 0.0849	R_1 = 0.0308 wR_2 = 0.0679	R_1 = 0.0486 wR_2 = 0.0776
Largest diff. peak and hole /e.Å^{-3}	0.30/-0.39	0.405 and -0.247	0.32 and -0.29

9. References

S1 H. Ackermann, J. Prue and G. Schwarzenbach, *Nature,* 1949, 723–724.

S2 C. M. Harris, T. N. Lockyer, R. L. Martin, R. L. Patil, E. Sinn and I. M. Stewart, *Aust. J. Chem.* **1969**, *22*, 2105–2126.